Chinese Chemical Letters 35 (2024) 109278

Contents lists available at ScienceDirect

Chinese Chemical Letters

journal homepage: www.elsevier.com/locate/cclet

Solid superacid catalysts promote high-performance carbon dots with narrow-band fluorescence emission for luminescence solar concentrators

Rui Cheng[a], Xin Huang[a], Tingting Zhang[a], Jiazhuang Guo[a], Jian Yu[a,*], Su Chen[a,b,*]

[a] State Key Laboratory of Materials-Oriented Chemical Engineering, College of Chemical Engineering, Nanjing Tech University, Nanjing 210009, China
[b] Jiangsu Key Laboratory of Fine Chemicals and Functional Polymer Materials, Nanjing 210009, China

ARTICLE INFO

Article history:
Received 17 September 2023
Revised 1 November 2023
Accepted 2 November 2023
Available online 4 November 2023

Keywords:
Carbon dots
Narrow full width at half maximum
Solid-state fluorescence
Luminescence solar concentrators
Photovoltaic conversion

ABSTRACT

Facile and efficient method for constructing carbon dots (CDs) with narrow full width at half maximum (FWHM) is a major challenge in the field, and researches on regulating the FWHM of CDs are also rare and scarce. In this work, we delved into the synthesis of CDs with narrow fluorescence emission FWHM (NFEF-CDs) in the *m*-phenylenediamine (*m*-PD)/ethanol system, utilizing solid superacid resin as catalyst with solvothermal method. The resulting NFEF-CDs exhibit a photoluminescent (PL) emission peak at 521 nm with a narrow FWHM of 41 nm, an absolute PL quantum yield (QY) of 80%, and display excitation-independent PL behavior. Through comprehensive characterization, we identified the protonation of edge amino on NFEF-CDs as the key factor in achieving the narrow FWHM. Subsequently, we validated the broad applicability of solid superacid resins as catalysts for synthesizing CDs with narrow FWHM in the *m*-PD/ethanol system. Finally, we utilized a self-leveling method to prepare NFEF-CDs film on the surface of poly(methyl methacrylate) (PMMA) substrate and investigated the solid-state fluorescence properties of NFEF-CDs as well as their performance as luminescence solar concentrator (LSC) for photovoltaic conversion. The results revealed that the as-prepared LSC exhibit an internal quantum efficiency (η_{int}) of 42.39% and an optical efficiency (η_{opt}) of 0.68%. These findings demonstrate the promising prospects of NFEF-CDs in the field of LSCs and provide a theoretical basis for their application in photovoltaic conversion.

In recent years, carbon dots (CDs) have emerged as promising candidates in the field of fluorescent nanomaterials, with significant potential for various applications [1–5]. CDs possess high photoluminescent (PL) quantum yields (QYs), excellent optical stability, tunable PL emission spectra, as well as desirable physicochemical properties such as excellent biocompatibility, low toxicity, and resistance to photobleaching [6–8]. These characteristics enable CDs to find applications in numerous fields, including catalysis, energy storage, displays, bioimaging, *etc.* [9–13]. However, compared to traditional semiconductor quantum dots, CDs still face challenges in terms of achieving high color purity in their optical properties [14].

To address this issue, numerous researchers have focused on investigating the regulation mechanisms and effective approaches to reduce the full width at half maximum (FWHM) of CDs. Recent studies have shown that factors influencing the FWHM of CDs can be summarized as their unique structure [15–18] and surface treatment [19–21]. Regarding the structure of CDs, Yang *et al.* proposed that the formation of π-conjugated systems from *N*-heterocycles or aromatic rings promotes the formation of a single emission center, thereby achieving a narrower FWHM [15]. Xiong *et al.* suggested that reducing oxygen-containing functional groups on CDs decreases the probability of electron-hole recombination captured by oxygen-related surface defects, leading to a narrower PL emission FWHM [16]. Fan *et al.* synthesized CDs with a triangular morphology and ultra-narrow emission bandwidth by using phloroglucinol as precursor. This unique structure ensures a high degree of delocalization and significantly reduces the electron-phonon coupling, resulting in high color purity of exciton emission [17]. Lei *et al.* indicated that a highly ordered graphite carbon structure within the CD framework is also crucial for achieving ultra-narrow PL emission [18]. In terms of surface treatment of CDs, Sargent *et al.* achieved the preparation of CDs with ultra-narrow emission bands by edge amino functionalization, which reduces the electron-phonon coupling probability [19]. Zhang *et al.* obtained fluorescent CDs with a FWHM of 24 nm by adjusting the pH value of the CD solution, thereby achieving

* Corresponding authors.
E-mail addresses: Yuj@njtech.edu.cn (J. Yu), chensu@njtech.edu.cn (S. Chen).

https://doi.org/10.1016/j.cclet.2023.109278
1001-8417/

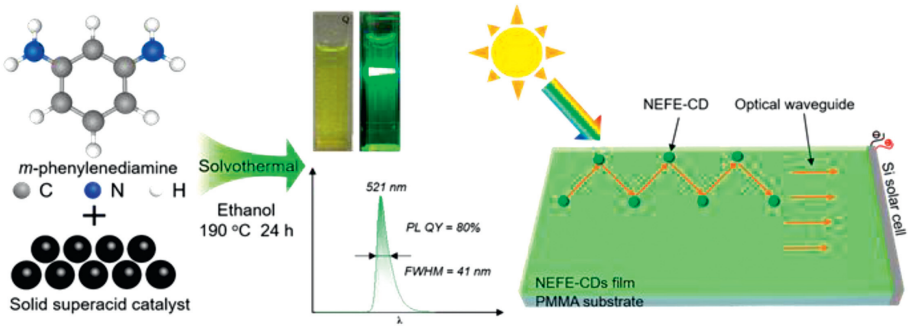

Fig. 1. Schematic diagram of synthesis and properties of NFEF-CDs and its application in LSC.

edge amino protonation treatment [20]. In our previous work, using *m*-phenylenediamine (*m*-PD) as the precursor, dilute sulfuric acid as the additive, and ethanol as the solvent, we synthesized green-emitting CDs with a FWHM of 46 nm and PL QY of 80% *via* one-step solvothermal method [21]. Dilute sulfuric acid promotes a highly graphitized structure of the CDs and reduces the presence of oxygen-containing functional groups on the surface.

Herein, we employed *m*-PD as the precursor and ethanol as the solvent to achieve the one-step synthesis of narrow fluorescence emission FWHM carbon dots (NFEF-CDs) (Fig. 1). To catalyze the reaction, we utilized a solid superacid resin, Amberlyst 70. The resulting NFEF-CDs exhibited green fluorescence with an emission peak at 521 nm, a FWHM of 41 nm, and an absolute PL QY of 80%. Experimental results demonstrated the pivotal role of the Amberlyst 70 catalyst in achieving the exceptional optical properties of the NFEF-CDs. Moreover, we found that various solid superacid resins can serve as effective catalysts for this reaction, providing valuable experimental references for the preparation of CDs with narrow FWHM. Notably, the NFEF-CDs exhibited remarkable solid-state fluorescence characteristics, making them suitable for photovoltaic applications such as luminescence solar concentrators (LSCs), where they demonstrated an impressive internal quantum efficiency (η_{int}) of 42.39% and an optical efficiency (η_{opt}) of 0.68%. This study not only provides a theoretical basis for the development of high-performance CDs with ultra-narrow fluorescence emission FWHM but also establishes important experimental groundwork for their application in energy conversion fields.

First, the morphology and structure of the obtained NFEF-CDs were characterized. Fig. 2a shows the transmission electron microscope (TEM) image of NFEF-CDs, demonstrating their excellent dispersibility and uniform morphology. Fig. S1 (Supporting information) presents the size distribution of the NFEF-CDs, which exhibits a normal distribution with an average size of 6.9 nm. Fig. 2b displays the high-resolution TEM (HRTEM) image of the NFEF-CDs, revealing their spherical shape and clear lattice spacing of 0.19 nm, corresponding to the (103) plane of graphite carbon [22], and the lattice diffraction pattern of NFEF-CDs confirms the typical graphite carbon structure. Atomic force microscopy (AFM) (Fig. 2c) further confirms the uniform dispersion of the NFEF-CDs with an average height of approximately 7 nm, consistent with the TEM results. The X-ray diffraction (XRD) spectrum (Fig. 2d) of NFEF-CDs shows a broad peak at 22°, corresponding to the (002) plane of graphite carbon [23]. The Fourier transform infrared (FT-IR) spectrum (Fig. 2e) analyzed the surface functional groups of NFEF-CDs. The FT-IR absorption peaks at 879 and 1379 cm^{-1} correspond to the bending vibrations of benzene rings and sp^3-hybridized C–H bonds, respectively [24,25]. The FT-IR absorption at 1046 and 1087 cm^{-1} represent the stretching vibration of C–O bonds, while the absorption at 1648 cm^{-1} corresponds to the stretching vibration of C=C bonds, and the absorption at 3320 cm^{-1} represents the stretching vibration of N–H bonds [26–28]. Specially, The FT-IR absorption at 2889 and 2932 cm^{-1} are attributed to the stretching vibration of $-NH_3^+$ [20]. X-ray photoelectron spectroscopy (XPS) analysis was conducted to further investigate the elemental characteristics of the NFEF-CDs' structure, revealing the presence of carbon, nitrogen, and oxygen elements (Fig. 2f). The C 1s spectrum (Fig. 2g) confirmed the presence of C–C/C=C (284.7 eV) and C–O/C–N (285.6 eV) [29]. The N 1s spectrum (Fig. 2h) indicated the presence of pyrrolic N (399.4 eV) [30] and pyridinic N (396.4 eV) [31] in NFEF-CDs. The O 1s spectrum (Fig. 2i) revealed the presence of C=O (532 eV) [32] and C–O (532.5 eV) [33] in NFEF-CDs.

Next, the optical properties of NFEF-CDs were characterized and discussed in detail. Fig. 3a shows the ultraviolet–visible (UV–vis) absorption and PL spectra of NFEF-CDs. The absorption spectrum exhibits two prominent peaks at 464 and 263 nm, corresponding to the n-π^* transition of the conjugated C=N or C=S bonds [34] and the π-π^* transition of C=C bonds [35]. The PL spectrum of NFEF-CDs reveals an emission peak at 521 nm with a FWHM of 41 nm. Notably, NFEF-CDs exhibit low-level reabsorption, indicating their potential application in the field of photovoltaics. Fig. 3b displays the PL spectra of NFEF-CDs under different excitation wavelengths, demonstrating their excitation-independent characteristics as the emission peak remains at 521 nm when the excitation wavelength ranges from 300 nm to 500 nm. Fig. 3c further highlights the changes in PL intensity of NFEF-CDs under different excitation wavelengths, showing higher PL intensity when excited at 470, 480, and 490 nm. Compared to traditional fluorescent CDs, the advantage of NFEF-CDs lies in their narrow FWHM. Fig. 3d illustrates the variation of the PL emission FWHM of NFEF-CDs with different excitation wavelengths. It can be observed that when the excitation wavelength is in the blue region (400–500 nm), the FWHM of NFEF-CDs' PL spectra is less than 50 nm, with a minimum value of approximately 41 nm. Compared to previous works in the field of green-emissive CDs, NFEF-CDs demonstrate significant advantages in optical properties, particularly regarding FWHM, which is superior to that of most CDs (Table S1 in Supporting information). Fig. 3e presents the PL decay curve of NFEF-CDs, which was fitted using a double-exponential function to obtain an average PL lifetime of 3.56 ns. Fig. 3f shows the absolute PL QY test curve of NFEF-CDs using anhydrous ethanol as the reference, yielding an absolute PL QY of 80%. In the experimental section, we conducted a detailed exploration of the optimal experimental parameters, including the mass of Amberlyst 70, reaction time, and reaction temperature. Fig. S2a (Supporting information) shows the PL spectra obtained by adding different masses of Amberlyst 70 catalyst at reaction temperature of 180 °C and reaction time of 24 h. Fig. S2b (Supporting information) illustrates the variation of PL emission peak positions and intensities with the Amberlyst 70 mass, indicating that the optimal mass of Amberlyst 70 is 1.2 g. Fig. S3 (Supporting information) depicts the PL spectra of the CDs and the changes in emission peak positions and intensities under different reaction times at a

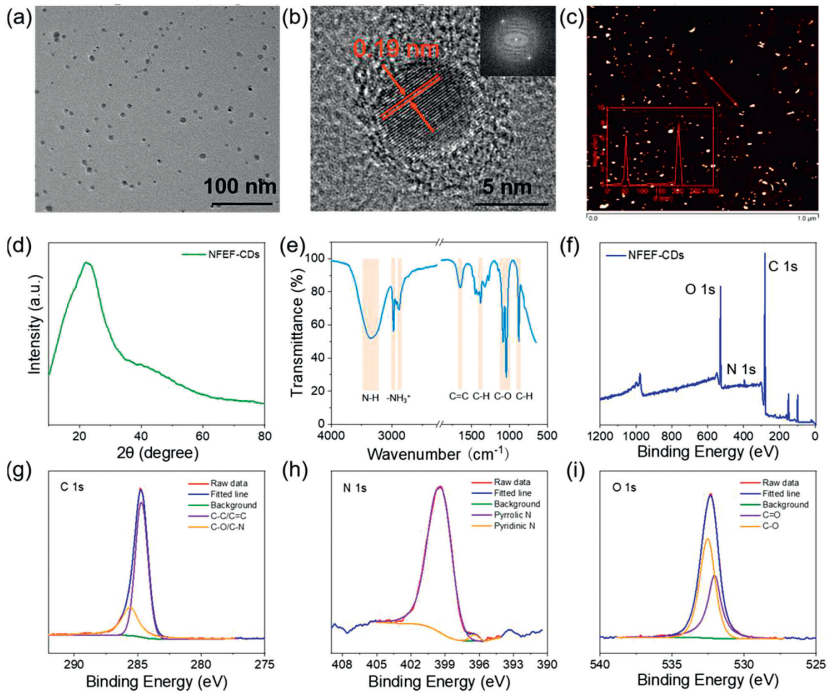

Fig. 2. (a) TEM image of NFEF-CDs. (b) HRTEM image of NFEF-CDs. Inset: diffraction pattern of NFEF-CD. (c) AFM image of NFEF-CDs. Inset: height profile of the selected line in AFM image. XRD pattern (d) and FT-IR curve (e) of NFEF-CDs. (f) XPS survey spectrum of NFEF-CDs, and the corresponding high-resolution (g) C 1s, (h) N 1s, (i) O 1s XPS spectra.

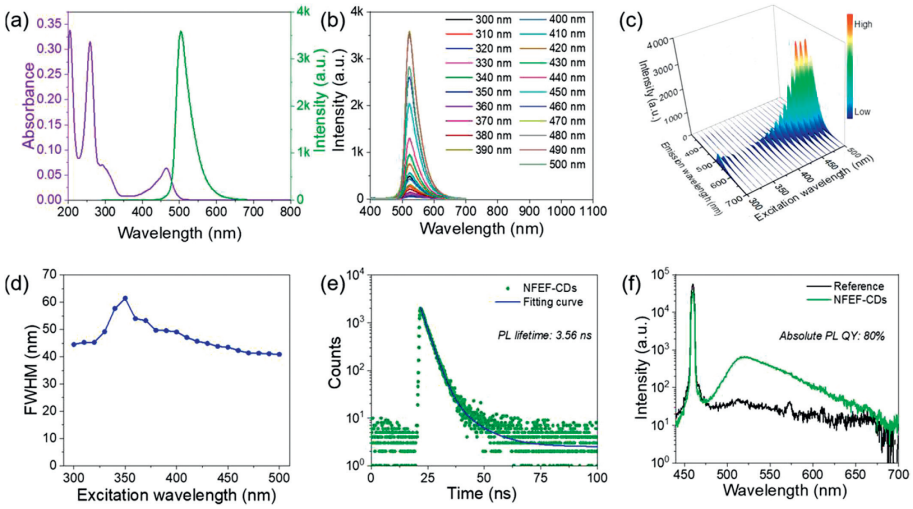

Fig. 3. (a) UV–vis absorption and PL spectra of NFEF-CDs. (b) PL spectra of NFEF-CDs with excitation wavelengths from 300 nm to 500 nm. (c) 3D PL mapping of NFEF-CDs. (d) The variation of FWHM under the different excitation wavelengths from 300 nm to 500 nm. (e) The time-resolved fluorescence decay curve of NFEF-CDs. (f) PL emission spectra used for measuring absolute PL QY.

Amberlyst 70 mass of 1.2 g and a reaction temperature of 180 °C. It reveals that the optimal reaction time is 24 h. Fig. S4 (Supporting information) presents the PL spectra of the CDs and the changes in PL emission peak positions and intensities at different reaction temperatures, with a Amberlyst 70 mass of 1.2 g and a reaction time of 24 h, indicating that the optimal reaction temperature is 190 °C. Furthermore, we verified the repeatability of the solid superacid catalyst in *m*-PD/ethanol system. Fig. S5 (Supporting information) shows the PL spectra of NFEF-CDs obtained using the Amberlyst 70 catalyst in the first reaction and after repeating the reaction once. The results demonstrate that the FWHMs of NFEF-CDs obtained from the two reactions remained nearly unchanged. However, the PL intensity of NFEF-CDs from the second reaction experienced a slight reduction, and the emission peak shifted from 521 nm to 519 nm. The shift of emission peak and slightly lower PL intensity might be attributed to a minor loss of catalyst after the first reaction, resulting in a decreased quantity of the catalyst available for the second reaction. In a word, in this reaction system, the solid superacid catalyst can be reused with maintained catalytic activity.

To investigate the mechanism behind the narrow PL emission FWHM and high PL QY of NFEF-CDs, *m*-PD based CDs (PD-CDs) without solid superacid were prepared using *m*-PD as the precursor. Fig. S6 (Supporting information) displays the PL spectrum of PD-CDs, exhibiting blue fluorescence with an emission peak at 445 nm, a FWHM of 120 nm, and a PL QY of 14%. Compared to NFEF-CDs, PD-CDs demonstrate a significant decrease in PL performance. The outstanding narrow FWHM of NFEF-CDs may be at-

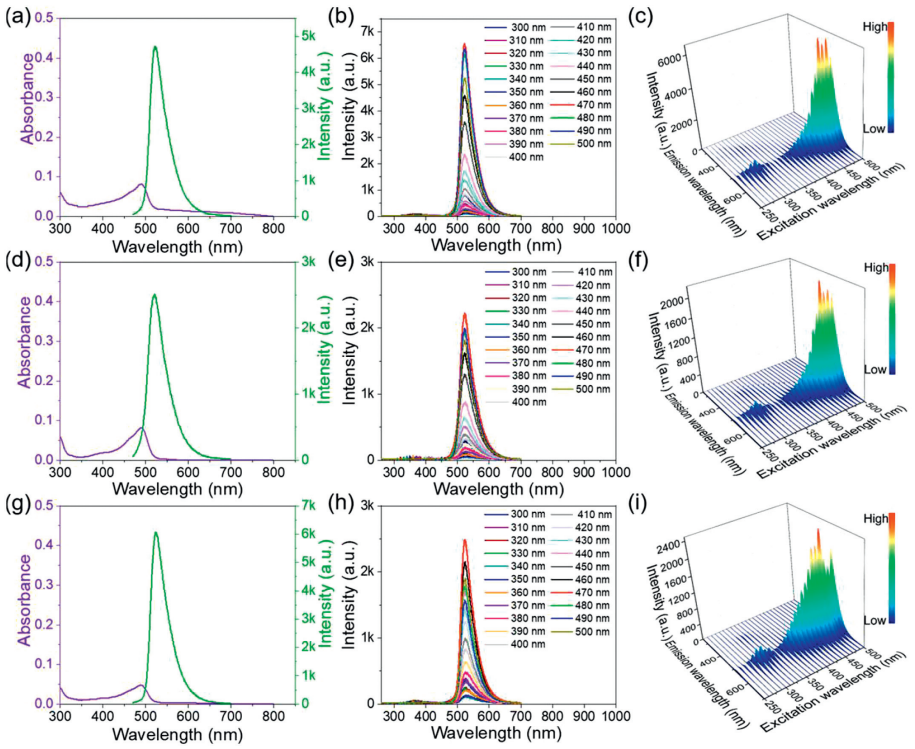

Fig. 4. UV–vis absorption and PL spectra (a, d, g), PL spectra with excitation wavelengths from 300 nm to 500 nm (b, e, h), 3D PL mapping (c, f, i) of NFEF-CDs-35WET, NFEF-CDs-36WET, and NFEF-CDs-40WET, respectively.

tributed to the strong acidity of Amberlyst 70, which promotes a higher degree of graphitization of the *m*-PD, reducing the number of oxygen-containing functional groups and resulting in delocalized wavefunctions and smaller bandgap fluctuations [36]. Zeta potential measurements were conducted on PD-CDs and NFEF-CDs (Fig. S7 in Supporting information), revealing zeta potentials of −14.6 mV and 0.52 mV, respectively. This indicates that Amberlyst 70 indeed alters the surface potential of NFEF-CDs and achieves edge amino protonation. Furthermore, the presence of $-NH_3^+$ was confirmed by FT-IR spectrum of NFEF-CDs.

To verify the practicality of preparing CDs with narrow PL emission FWHM under the effective catalytic action of solid superacid in the *m*-PD/ethanol system, various solid superacid catalysts were selected in the experiments. Similar to Amberlyst 70, Amberlyst 35WET, Amberlyst 36WET, and Amberlyst 40WET resins were chosen as solid superacid catalysts. Fig. 4a shows the PL and UV–vis absorption spectra of the CDs (abbreviated as NEFE-CDs-35WET) prepared using Amberlyst 35WET as the catalyst. The absorption peak is located at 490 nm, while the PL emission peak is at 523 nm with a FWHM of 44 nm. Like NEFE-CDs, NEFE-CDs-35WET also exhibits excitation-independent characteristics when the excitation wavelength ranges from 300 nm to 500 nm (Fig. 4b). The 3D PL mapping clearly shows that NEFE-CDs-35WET has higher PL intensity when excited at wavelengths between 470 nm and 490 nm (Fig. 4c). Similarly, CDs prepared using Amberlyst 36WET as the catalyst (abbreviated as NEFE-CDs-36WET) show an absorption peak at 490 nm and a PL emission peak at 521 nm, with a FWHM of 49 nm (Fig. 4d), also demonstrating excitation-independent behavior, and the PL intensity is relatively higher at the excitation wavelength of 470 nm (Figs. 4e and f). CDs prepared with Amberlyst 40WET catalyst (abbreviated as NEFE-CDs-40WET) display an absorption peak at 490 nm and a PL emission peak at 523 nm, with a FWHM of 43 nm, showing excitation-independent behavior and optimal excitation wavelength is 470 nm (Figs. 4g–i). These results indicate that in the *m*-PD/ethanol system, the Amberlyst series of solid superacid resins can serve as effective catalysts for preparing CDs with narrow PL emission FWHM. In this work, we attempted to synthesize CDs using *o*-phenylenediamine (*o*-PD) and *p*-phenylenediamine (*p*-PD) as precursors with Amberlyst 70 as the catalyst. The PL spectra, as shown in Fig. S8 (Supporting information), reveal that CDs prepared using *o*-PD and *p*-PD exhibit lower PL intensities and broader FWHMs (greater than 100 nm). This indicates that solid superacid catalysts are currently only applicable to the *m*-PD/ethanol system.

We also explored the solid-state fluorescence performance of NEFE-CDs and their application in LSCs. As the possible complements to standard photovoltaic equipment, LSCs are new type of device that can be used for sunlight collection and conversion [37,38]. Typically, LSCs are prepared by coating fluorescent materials onto transparent polymer substrates or glass surfaces. When incident light strikes the surface of LSCs, the fluorescent materials absorb the light and convert it into longer-wavelength light, which is then randomly emitted. Due to the higher refractive index of the LSCs compared to air, most emitted photons undergo total internal reflection within the LSCs and are guided towards the edges of the LSCs [39]. By covering photovoltaic cells on the edges of the LSCs, continuous electricity generation can be achieved. In this work, we mixed NEFE-CDs uniformly with a transparent optical coating and applied it as a self-leveling coating on the surface of poly(methyl methacrylate) (PMMA) to obtain NEFE-CDs@PMMA LSC. Fig. 5a shows photographs of NEFE-CDs@PMMA LSC (150 mm × 50 mm × 5 mm) under sunlight and 365 nm UV light. It can be observed that after coating with a layer of NEFE-CDs, NEFE-CDs@PMMA LSC retains good transparency and exhibits a pale yellow color. Bright green fluorescence can be observed under UV light, with higher brightness at the edges. The PL spectrum of NEFE-CDs@PMMA LSC (Fig. 5b) shows an emission peak at 532 nm with a FWHM of 50 nm. We investigated the PL spectra and intensity changes of NEFE-CDs at different optical distances in NEFE-CDs@PMMA LSC. The experimental setup involved

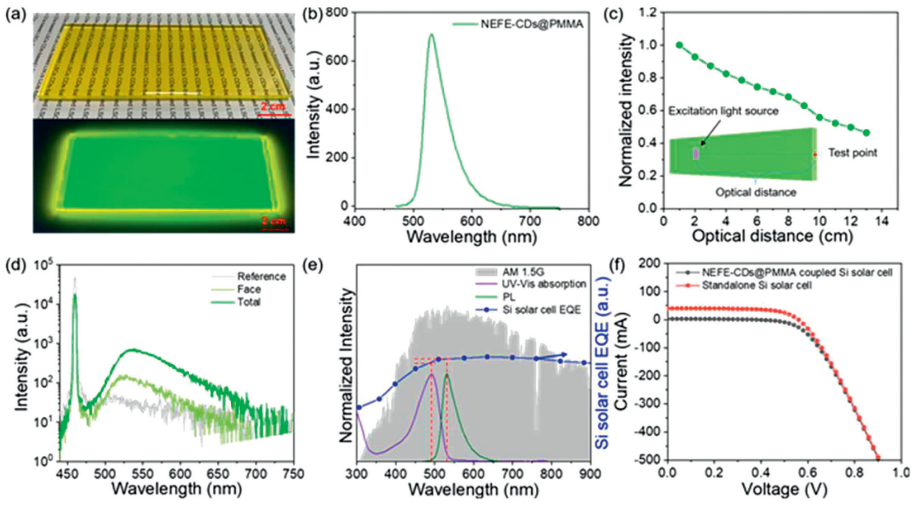

Fig. 5. (a) Photographs of NEFE-CDs@PMMA LSC taken under daylight (upper) and 365 nm UV light (lower). (b) PL spectrum of NEFE-CDs@PMMA LSC. (c) PL intensities as a function of propagation lengths in the NEFE-CDs@PMMA LSC. Inset: the schematic diagram of distance-related PL intensity test method. (d) PL curves of NEFE-CDs@PMMA LSC for measuring overall PL QY and surface PL QY. (e) Absorption (purple) and PL (green) spectra of NEFE-CDs@PMMA LSC along with the AM 1.5 G solar spectrum (gray) and a typical Si solar cell EQE spectrum (blue). (f) The *I-V* curves of the Si solar cell coupled with the edge of an LSC and standalone Si solar cell.

placing the testing probe of fiber optic spectrometer at the edge of the horizontally placed NEFE-CDs@PMMA LSC and moving the excitation light source (365 nm) on the top surface of the LSC to record the corresponding PL spectra at different optical distances (Fig. 5c). The PL intensity of NEFE-CDs gradually decreased with increasing optical distance, due to energy loss from reabsorption in the LSC [40]. When the distance increased to 13 cm, the PL intensity remained at 46.5% of the initial value. Fig. S9 (Supporting information) shows the corresponding PL spectra for the distances in Fig. 5c. It can be observed that the PL peak position of NEFE-CDs remains unchanged with increasing optical distance, which is attributed to the excitation-independent PL characteristics of NEFE-CDs. Additionally, we investigated the light-collecting capability of NEFE-CDs@PMMA LSC. Taking a square-faced NEFE-CDs@PMMA LSC (50 mm × 50 mm × 5 mm) as the study sample (Fig. S10 in Supporting information), the geometric factor (G) was calculated using the following Eq. 1 [39]:

$$G = \frac{A_{top}}{A_{edge}} \tag{1}$$

where A_{top} and A_{edge} represent the top surface area and edge surface area of LSC, respectively. The calculated value of G was 10. Previous reports primarily evaluated the light-collecting ability of LSCs based on their internal optical quantum efficiency (η_{int}), calculated using the following Eq. 2 [41]:

$$\eta_{int} = \frac{\text{no. of edge} - \text{emitted photons}}{\text{no. of total absorbed photons}} = PLQY_{total} - PLQY_{face} \tag{2}$$

where $PLQY_{total}$ represents the overall PLQY of LSC (including top, bottom, and edge surfaces), and $PLQY_{face}$ represents the PLQY of the top and bottom surfaces of LSC (Fig. S11 in Supporting information). Fig. 5d shows the curves of $PLQY_{total}$ and $PLQY_{face}$ for NEFE-CDs@PMMA LSC, with the values of 51.15% and 8.76%, respectively, resulting in η_{int} of 42.39%, which is relatively high compared to previous studies in the field of CDs (Table S2 in Supporting information). Fig. 5e displays the AM 1.5 G spectrum, the absorption and emission spectra of NEFE-CDs@PMMA LSC, and the external quantum efficiency (EQE) variation of a commercial Si solar cell. It is evident that the absorption peak position of NEFE-CDs@PMMA LSC corresponds to the wavelength region with higher light intensity in the AM 1.5 G spectrum. On the other hand, the emission peak position has a higher EQE corresponding to the Si solar cell compared to the absorption peak position. Consequently, Si solar cell coupled with NEFE-CDs@PMMA LSC will exhibit improved photoelectric conversion efficiency. Optical efficiency (η_{opt}) is another important performance parameter of LSCs, representing the ratio of output power at the edges of LSC to input power on the surface. It can be easily calculated by coupling Si solar cell to the edge of LSC, with the following Eq. 3 [42]:

$$\eta_{opt} = \frac{I_{lsc}}{I_{sc} \times G} \tag{3}$$

where I_{lsc} and I_{sc} represent the short-circuit current of LSC coupled with Si solar cell and the standalone Si solar cell under direct illumination, respectively, and G is the geometric factor. Fig. 5f shows the *I-V* curves of Si solar cell and Si solar cells coupled with NEFE-CDs@PMMA LSC, with short-circuit currents of 2.65 and 38.9 mA, respectively, leading to an η_{opt} of 0.68% for NEFE-CDs@PMMA LSC. The above results indicate that NEFE-CDs possess excellent solid-state fluorescence performance and their low reabsorption characteristics make them a promising material for fabricating LSCs.

In conclusion, we have developed a straightforward method for synthesizing CDs with narrow FWHM. In the *m*-PD/ethanol system, using solid superacid resin as the catalyst, we successfully obtained green-emitting NFEF-CDs with an emission peak at 521 nm, a narrow FWHM of 41 nm, and an absolute PL QY of 80% by solvothermal method. Through a series of experiments, we demonstrated the universality of various solid superacid resins in this system, all of which can produce green-emitting CDs with narrow FWHM. Combined with FT-IR and zeta potential characterization, we attributed the achievement of narrow FWHM to the edge amino protonation on the surface of NFEF-CDs. Furthermore, we utilized a self-leveling method to coat a layer of NFEF-CDs on the surface of PMMA substrate, thereby creating a CDs-based LSC for photovoltaic devices. The prepared NFEF-CDs@PMMA LSC not only exhibited excellent solid-state fluorescence but also achieved a η_{int} of 42.39% and a η_{opt} of 0.68%. These results demonstrate the potential application value of NFEF-CDs in the field of LSCs.

Declaration of competing interest

The authors declare that they have no known competing financial interests or personal relationships that could have appeared to influence the work reported in this paper.

Acknowledgments

This work was supported by the National Natural Science Foundation of China (No. 22308161), the Jiangsu Funding Program for Excellent Postdoctoral Talent (No. 2022ZB369), Priority Academic Program Development of Jiangsu Higher Education Institutions (PAPD).

Supplementary materials

Supplementary material associated with this article can be found, in the online version, at doi:10.1016/j.cclet.2023.109278.

References

[1] L. Đorđević, F. Arcudi, M. Cacioppo, M. Prato, Nat. Nanotechnol. 17 (2022) 112–130.
[2] B.Y. Wang, G.I.N. Waterhouse, S.Y. Lu, Trends Chem. 5 (2023) 76–87.
[3] H.L. Wang, L. Ai, H.Q. Song, et al., Adv. Funct. Mater. 33 (2023) 2303756.
[4] X. Yang, X. Li, B.Y. Wang, et al., Chin. Chem. Lett. 33 (2022) 613–625.
[5] M.Y. Fang, B.Y. Wang, X.L. Qu, et al., Chin. Chem. Lett. 35 (2024) 108423.
[6] J.T. Li, W.J. Fu, X.Y. Zhang, et al., Carbon 208 (2023) 208–215.
[7] X.Q. Qu, C.X. Gao, L. Fu, et al., ACS Appl. Mater. Interfaces 15 (2023) 18608–18619.
[8] N. Li, X.Z. Dong, X.G. Lv, et al., Chem. Commun. 59 (2023) 4475–4478.
[9] Y.Q. Zhang, J.P. Wang, L. Wang, et al., Adv. Mater. 35 (2023) 2302536.
[10] W.D. Li, Y. Liu, B.Y. Wang, et al., Chin. Chem. Lett. 30 (2019) 2323–2327.
[11] Y.F. Zhou, D. Benetti, X. Tong, et al., Nano Energy 44 (2018) 378–387.
[12] P.D. Zhu, X.L. Zhao, Q.Y. Zhu, et al., Chem. Eng. J. 470 (2023) 144042.
[13] J.Y. Chen, X.K. Zou, W. Li, et al., Adv. Opt. Mater. 10 (2022) 2200851.
[14] R.J. Chen, Z.B. Wang, T. Pang, et al., Adv. Mater. 35 (2023) 2302275.
[15] J.J. Liu, Y.J. Geng, D.W. Li, et al., Adv. Mater. 32 (2020) 1906641.
[16] H. Ding, J.S. Wei, P. Zhang, et al., Small 14 (2018) 1800612.
[17] F.L. Yuan, T. Yuan, L.Z. Sui, et al., Nat. Commun. 9 (2018) 2249.
[18] J. Chen, W.R. Liu, Y. Li, et al., Chem. Eng. J. 428 (2022) 131168.
[19] F. Yuan, Y.K. Wang, G. Sharma, et al., Nat. Photonics 14 (2019) 171–176.
[20] Q. Zhang, R.Y. Wang, B.W. Feng, X.X. Zhong, K. Ostrikov, Nat. Commun. 12 (2021) 6856.
[21] R. Cheng, T. Zhang, X. Huang, J. Yu, Chin. Chem. Lett. 35 (2024) 108763.
[22] S. Zhang, M. Gao, Y. Zhai, et al., J. Colloid Interface Sci. 622 (2022) 662–674.
[23] Z.Y. Wang, H. Liao, H. Wu, et al., Anal. Methods 7 (2015) 8911–8917.
[24] B.E. Kwak, H.J. Yoo, D. Kim, Adv. Opt. Mater. 7 (2019) 1900932.
[25] A. Basu, A. Suryawanshi, B. Kumawat, et al., Analyst 140 (2015) 1837–1841.
[26] I. Perelshtein, N. Perkas, S. Rahimipour, A. Gedanken, Nanomaterials 10 (2020) 1384.
[27] J. Chen, H. Zhao, Z. Li, X. Zhao, X. Gong, Energy Environ. Sci. 15 (2022) 799–805.
[28] K. Sato, R. Sato, Y. Iso, T. Isobe, Chem. Commun. 56 (2020) 2174–2177.
[29] S.Y. Tao, S.Y. Lu, Y.J. Geng, et al., Angew. Chem. Int. Ed. 57 (2018) 2393–2398.
[30] W.Y. Shi, R.X. Wang, J. Liu, et al., Angew. Chem. Int. Ed. 62 (2023) e202303063.
[31] K. Arkin, Y.X. Zheng, J.W. Hao, S.Y. Zhang, Q.K. Shang, ACS Appl. Nano Mater. 4 (2021) 8500–8510.
[32] A. Kolanowska, D. Lukowiec, M. Krzywiecki, J. Bok-Badura, S. Boncel, Chem. Commun. 59 (2023) 7659–7662.
[33] Q. Zhang, F. Wang, R. Wang, et al., Adv. Sci. 10 (2023) 2207566.
[34] H.W. Tian, K. Shen, X.Y. Hu, L.A. Qiao, W.T. Zheng, J. Alloy. Compd. 691 (2017) 369–377.
[35] W.J. Chen, J. Fan, X.X. Wu, et al., New J. Chem. 45 (2021) 5114–5120.
[36] G.H. Oh, B.S. Kim, Y.J. Song, S. Kim, Appl. Surf. Sci. 605 (2022) 154690.
[37] Y.M. You, X. Tong, W.H. Wang, et al., Adv. Sci. 6 (2019) 1801967.
[38] M.G. Debije, R.C. Evans, G. Griffini, Energy Environ. Sci. 14 (2021) 293–301.
[39] Y.X. Li, P. Miao, W. Zhou, X. Gong, X.J. Zhao, J. Mater. Chem. A 5 (2017) 21452–21459.
[40] H.G. Zhao, R.J. Sun, Z.F. Wang, et al., Adv. Funct. Mater. 29 (2019) 1902262.
[41] J.Z. Guo, Y.S. Lu, A.Q. Xie, et al., Adv. Funct. Mater. 32 (2022) 2110393.
[42] J.J. Wu, J.Y. Tong, Y. Gao, et al., Angew. Chem. Int. Ed. 59 (2020) 7738–7742.